October 2003

High-sensitivity photoacoustic leak testing

Eric Huang
University of Michigan

David R. Dowling
University of Michigan

Timothy Whelan
Honeywell Federal Manufacturing & Technologies

John L. Spiesberger
University of Pennsylvania, johnsr@sas.upenn.edu

Copyright ASA. Reprinted from *Journal of the Acoustical Society of America*, Volume 114, Issue 4, October 2003, pages 1926-1933 .
Publisher URL: http://dx.doi.org/10.1121/1.1605386

High-sensitivity photoacoustic leak testing

Abstract
The photoacoustic effect may be exploited for the detection and localization of gas leaks from otherwise sealed components. The technique involves filling the test component with a tracer gas, and radiating the component to produce photoacoustic sound from any leak site where tracer gas is present. This paper describes demonstration experiments utilizing 10.6-μ radiation from a carbon-dioxide laser and sulfur hexafluoride as a tracer gas for photoacoustic leak testing at leak rates between 6×10^{-5} cm^3/s (1 cm^3 in 4.6 h) and 5×10^{-9} cm^3/s (1 cm^3 in 6.3 years). The technique may reach or exceed the capabilities of the most sensitive commercial leak test systems using helium mass-spectrometers. In addition, comparison of the measured results to a simple scaling law suggests that tracer gas cloud geometry influences the photoacoustic signal amplitude.

High-sensitivity photoacoustic leak testing

Eric Huang and David R. Dowling[a)]
Department of Mechanical Engineering, University of Michigan, Ann Arbor, Michigan 48109-2133

Timothy Whelan
Honeywell Federal Manufacturing & Technologies, LCC, P.O. Box 419159, Kansas City, Missouri 64141-6159

John L. Spiesberger
Department of Earth and Environmental Science, University of Pennsylvania, Philadelphia, Pennsylvania 19104-6316

(Received 27 January 2003; revised 25 June 2003; accepted 14 July 2003)

The photoacoustic effect may be exploited for the detection and localization of gas leaks from otherwise sealed components. The technique involves filling the test component with a tracer gas, and radiating the component to produce photoacoustic sound from any leak site where tracer gas is present. This paper describes demonstration experiments utilizing 10.6-μ radiation from a carbon-dioxide laser and sulfur hexafluoride as a tracer gas for photoacoustic leak testing at leak rates between $6\times10^{-5}\,\mathrm{cm}^3/\mathrm{s}$ (1 cm^3 in 4.6 h) and $5\times10^{-9}\,\mathrm{cm}^3/\mathrm{s}$ (1 cm^3 in 6.3 years). The technique may reach or exceed the capabilities of the most sensitive commercial leak test systems using helium mass-spectrometers. In addition, comparison of the measured results to a simple scaling law suggests that tracer gas cloud geometry influences the photoacoustic signal amplitude.
 [DOI: 10.1121/1.1605386]

PACS numbers: 43.38.Zp, 43.35.Ud, 43.60.Gk [AJZ]

I. INTRODUCTION

Photoacoustics is the generation of sound due to unsteady heating of a photoactive material—gas, liquid, or solid—by an unsteady source of light or invisible electromagnetic radiation. Over the last decade or so, gas-phase photoacoustics has been developed into a noncontacting means of detecting and locating small gas leaks on the exterior surfaces of components that are intended to be sealed. Although implementations may be different, photoacoustic leak test systems all rely on the same basic steps. First, the part under test is charged with a photoactive tracer gas (typically sulfur hexafluoride, SF_6) to a pressure greater than the local ambient pressure so that a cloud or plume of tracer gas forms adjacent to any unintended leak. Next, the component under test is scanned with a radiation source (typically a carbon dioxide, CO_2, laser) having a wavelength tuned to an absorption line of the photoactive gas (10.6 μ for SF_6). When a tracer gas plume is illuminated, photoacoustic sound is generated. Recordings of this sound can be analyzed to detect and locate the tracer gas plume when the test geometry and environment are known. Here, the tracer gas plumes are detected and localized, not the actual physical defect in the part that leads to an unintended gas pathway. However, for the volumetric leak rates of interest here ($\sim10^{-4}\,\mathrm{cm}^3/\mathrm{s}$ and lower), gas-phase diffusive transport ensures that the highest tracer gas concentrations will only occur at the location where tracer gas molecules emerge from the test component's surface.

Photoacoustic leak testing has advantages in sensitivity, speed, ease of implementation, and robustness compared to other leak test technologies for leak rates of $\sim10^{-4}\,\mathrm{cm}^3/\mathrm{s}$ and lower. It can be implemented at room temperature and pressure. Photoacoustic leak testing requires neither the complex high-vacuum system typically essential for helium-mass spectrometry (HeMS), nor the use of potentially hazardous chemicals like the ammonia-phenolphthalein method. Unlike dunk tanks and soap film systems, it is remote and noncontacting. It is more sensitive than pressure decay measurements or backscatter absorption systems, and is more robust (less likely to be fouled and much less operator dependent) than sniffer-based systems. In addition to the other listed advantages, photoacoustic leak tests can be completed in a matter of seconds for phone-book size components. Larger objects can be tested with scaled up versions of the test setup described here. The main liabilities of photoacoustic leak testing are its reliance on potentially dangerous laser radiation and its inability to accurately detect or locate leaks lying on interior or shadowed surfaces that cannot be illuminated.

The experimental results in this paper show that photoacoustic leak testing can be conducted at sensitivities that rival or possibly exceed that available from leak test systems based on HeMS, the method most utilized for sensitive testing in commercial technology. Helium mass spectrometry has been used for the detection of small leaks since World War II (Dushman and Lafferty, 1962) and is now used pervasively in manufacturing due to its high sensitivity, $10^{-10}\,\mathrm{cm}^3/\mathrm{s}$ or better (see Rasmussen and Jeppesen, 1998), relatively low cost, and good reliability. As of this writing, some commercial manufacturers (for example, Alcatel and BOC Edwards) are advertising HeMS systems capable of detecting leaks into the 10^{-12}-cm^3/s range and many others advertise systems capable of detecting leaks in the

a)Author to whom correspondence should be addressed. Electronic mail: drd@engin.umich.edu

10^{-11}-cm^3/s range. A good technical description of HeMS is given in Hablainian (1997). In addition to addressing sensitivity limits, the present results appear to defy a simple diffusive-transport scaling law for photoacoustic signal amplitudes as the leak rate decreases.

The main advantage of photoacoustic leak testing is that it allows small leaks, $10^{-5}\,cm^3/s$ or smaller, to be detected and located quickly. By comparison, locating leaks of such low flow rates with helium mass spectrometry is a time consuming, heavily operator-dependent process. There are two methods used to locate the leak with helium mass spectrometry. In the first method, the item of interest is filled with helium (or a mixture of helium and another gas) and a wand or sniffer is passed over the surface of the item. The wand is usually a tube with a small diameter hole that draws in gas which then passes through a tube into the mass spectrometer. In the second method, the item is connected to the mass spectrometer and a vacuum is created inside the unit. The operator then sprays the outside of the item with a slow flow of helium and watches the mass spectrometer for an indication of its presence. Due to the length of time necessary to perform these tests and the skill level required of the operators, these methods are frequently employed only after other tests have indicated a leak exists somewhere on the item.

Photoacoustic leak testing was first reported in McRae and Dewey (1992) and in McRae (1994), and is similar to work done on remote detection and ranging of gas clouds (Brassington, 1982). Since then commercial developments of the technique have seen it extended to include signal-to-noise ratio improvements via proper laser-scanning frequency selection (Olender *et al.*, 1998a), multiple laser beams (Olender *et al.*, 1998b), enclosures to improve signal characteristics (Schroff and Stetter, 1999), multiple microphones for acoustic localization (Yonak and Dowling, 2001), and multiple laser wavelengths for background noise assessment (Veronesi *et al.*, 2001). A general audience description of the approach followed here is available in Sharke (2000) with more detailed accounts provided in Yönak and Dowling (1999, 2002). The current results differ from these prior efforts in their emphasis on increased sensitivity.

II. EXPERIMENTAL SETUP

The experimental setup was nearly the same as for the cylindrical geometry leak tests described in Yönak and Dowling (2002) except that the optical and acoustic path lengths were shorter, 12 microphones were used instead of four, and a CO_2 laser capable of delivering a nominal 145 W, instead of the previously utilized 12 W, provided the input radiation. All experiments were conducted on an optical tabletop in a laboratory environment with painted cinder block walls and tiled floor.

The radiation source used in these experiments was a DeMaria ElectroOptics Systems, Inc. (DEOS) LC-100NV carbon dioxide (CO_2) laser. Its output power was controlled via pulse width modulation from a DEOS PC-1 controller and was measured using a SYNRAD PowerWizard™ PW-250 hand held laser power meter. A NESLAB M75 STD 208/60 PD2 chiller kept the laser head and power supply at 20 °C. A rotating 12-sided polygonal mirror assembly (Lincoln Laser Model DT-12-200-028) was used to repetitively sweep the incoming CO_2 laser through a plane lying parallel to, and 125 mm above, the optical tabletop. The rotational speed of the polygonal mirror assembly (18750 rpm) was set by a Lincoln Laser MC-5 motor controller, and the electrical power to the rotating mirror motor was supplied by an Acopian Model A48HT600 48 V dc power supply. For safety purposes, a coated ZnSe flat from II-VI Optics was used to combine and co-align the invisible and potentially dangerous CO_2 laser beam with a visible and relatively harmless 5 mW red He–Ne laser beam.

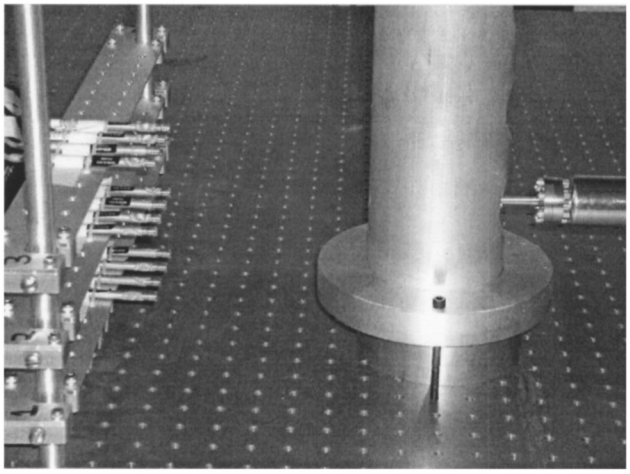

FIG. 1. Picture of the experimental test geometry. The 12-microphone array appears on the left and the vertical test cylinder on the right. The leak is located at the left edge of the test cylinder at the height of the SF_6 canister shown at the right edge of the picture. The spacing between holes in the optical tabletop is 25.4 mm in each direction.

A brushed aluminum cylinder having a 10-cm diameter provided the test surface on which the calibrated SF_6 leaks were mounted. The axis of this test cylinder was vertical and perpendicular to the tabletop (see Fig. 1). The test surface of the cylinder was the semi-circle determined by the intersection of the CO_2-laser scan plane with the cylinder. The six calibrated leaks in this study were manufactured by Vacuum Technology, Inc. and ranged in rate from $6.0\times10^{-5}\,cm^3/s$ down to $5.0\times10^{-9}\,cm^3/s$. The front 25% of a SF_6-reservoir canister for one of these leaks is shown at the right edge of Fig. 1. The leaking gas was brought to the test surface with special high-vacuum fittings and a leak cap having a diagonal hole. This hole forced the leaking SF_6 to escape from a known location without letting the CO_2 laser beam shine into the gas volume trapped between the leak orifice and the outside of the leak cap (see Fig. 2).

Twelve 7.6-mm-diam condenser microphones (Brüel and Kjaer type 4939-A011) were used to record the photoacoustic sounds created by the swept laser beam as it passed through the SF_6 gas cloud formed at the opening of the leak cap. The microphones were placed 152 mm from the leak in a 3 by 4 array as shown in Fig. 1. The microphone rows were 57, 108, and 159 mm above the tabletop, and the horizontal spacing between microphones was 25.4 mm. In Fig. 1, the invisible CO_2-laser beam emerges between the upper two

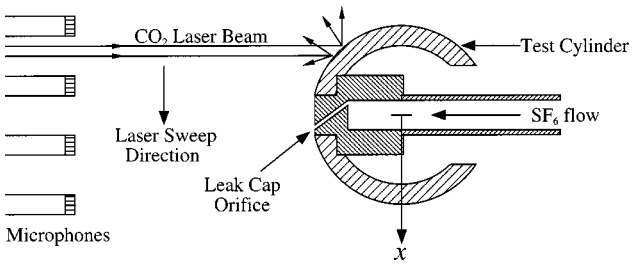

FIG. 2. Schematic top view of the experimental test geometry.

rows of microphones and traverses the picture from left to right, hitting the test cylinder at the height of the leak. The microphone signals were amplified using three four-channel Brüel and Kjaer NEXUS Type 2690 microphone conditioning amplifiers to an output sensitivity of 316 mV/Pa, high-pass filtered above 3 kHz with three four-channel Krohn-Hite Model 3384 active filters with an output gain of 10 dB, digitized with 12-bit resolution at 400 kHz using National Instruments data acquisition hardware, and stored in a laboratory PC computer running Labview® software. The nominal experimental bandwidth was 3 to ~80 kHz, the upper limit being determined by the roll-off of the microphones with their protection grids in place.

The digitized microphone signals were Fourier analyzed and comb-filtered to select the signal frequencies. Bartlett matched-field processing (MFP), computed along the intersection of the laser scan plane and the front of the test cylinder (the semi-circular test surface), was conducted at each signal frequency using the tabletop as a hard reflecting surface to detect and locate the various leaks. These single-frequency Bartlett ambiguity surfaces were incoherently averaged across 16 signal frequencies from 15 to 75 kHz to obtain the final broadband Bartlett ambiguity-surface results presented in the next section. For the present purposes, these final Bartlett MFP results can be interpreted as indicating the likelihood of a leak lying at a particular location. When a peak in the Bartlett MFP output rises well above the noise level, a leak is detected and its acoustically determined location is the position of the ambiguity-surface peak. Bartlett MFP is described in Jensen *et al.* (1994) and has been used in prior leak test studies (see Yönak and Dowling, 1999, 2002).

III. RESULTS

For simplicity, all of the results reported here are from leaks centered on the swept laser beam's path across the cylinder ($x=0$). Figure 3 shows Bartlett MFP output on the vertical axis vs x—the horizontal Cartesian coordinate perpendicular to the test cylinder's axis and the line connecting the axis of the spinning mirror to the test cylinder axis—for the smallest leak in this study at CO_2 laser power levels between 0 and 140 W. Here $x=\pm 5$ cm corresponds to the edges of the test cylinder when it is viewed from the microphone array. The main feature of this figure is the prominence of the Bartlett MFP peak at $x=0$ for all nonzero laser powers. Furthermore, the peaks are monotonically increasing in height with increasing laser power. These results show that 5×10^{-9} cm^3/s of SF_6, which corresponds to approximately 1 cm^3 every 6 years, does indeed produce measurable photoacoustic sound. It should be mentioned that the 5×10^{-9} cm^3/s of SF_6 was the smallest leak for which a supplier was found. This leak was also at the NIST traceable detectable limit of the supplier's capabilities for SF_6.

Figures 4 and 5 show how the Bartlett MFP results vary with leak rate for laser powers of 10 and 140 W. Here, the plug and cylinder test cases involve a blank leak cap inserted into the test cylinder in place of a calibrated leak. Thus, these test cases represent the background noise signature of this experimental geometry at nominal laser powers of 10 and 140 W. In all cases shown in Figs. 4 and 5, the leaks are indicated by a substantial peak in the Bartlett output near $x=0$, which exceeds the background peak obtained without a leak at the same laser power. The minor misalignment of the signal peaks from $x=0$, about ± 1 mm, and the limitation on the height (~0.7) of the Bartlett peaks for the larger leaks were traced to a minor synchronization problem in the

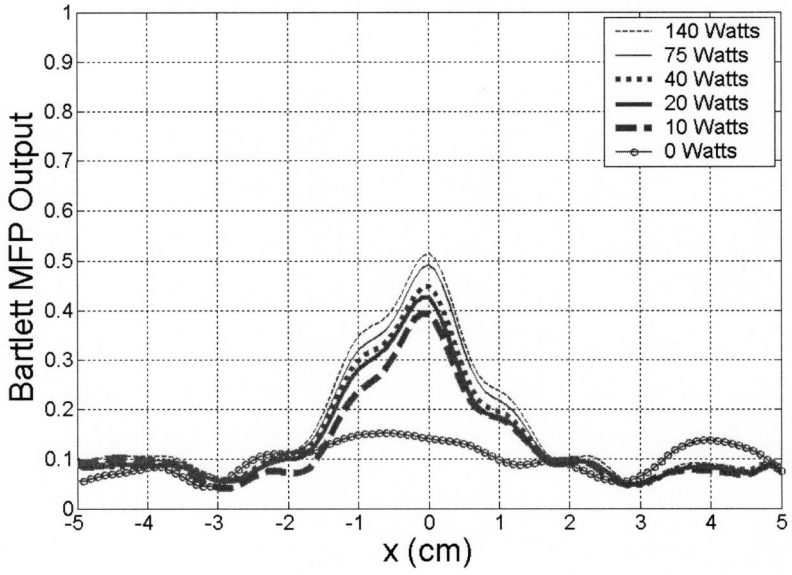

FIG. 3. Bartlett MFP output along the surface of the test cylinder versus horizontal distance for the 5.0×10^{-9} cm^3/s SF_6 leak at laser powers from zero to 140 W.

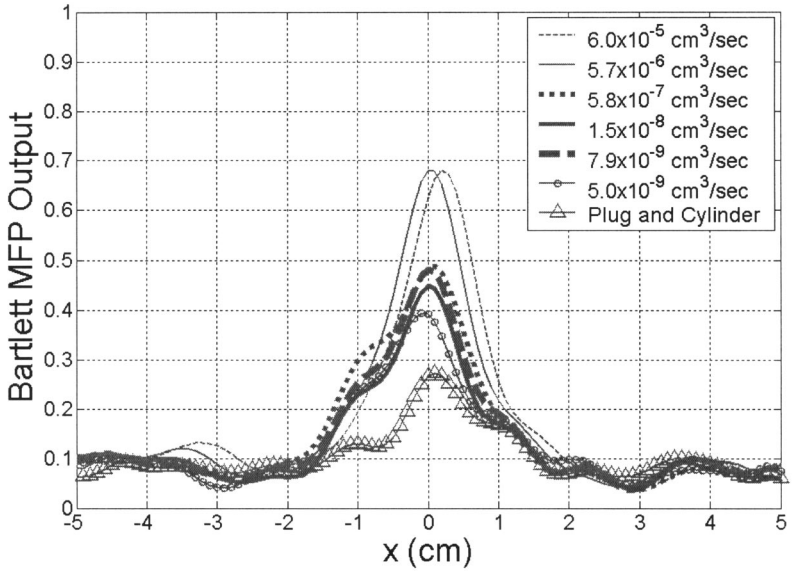

FIG. 4. Bartlett MFP output along the surface of the test cylinder versus horizontal distance for the various SF_6 leak rates at laser a laser power of 10 W. The "plug and cylinder" case represents background noise because it involves the entire experiment except no leak is present.

microphone-signal digitization system. Thus, these imperfections are artifacts of the experimental setup. Overall, Figs. 4 and 5 demonstrate that better results are achieved at higher laser powers, and that even the smallest leak of this study exceeds the background noise (the plug and cylinder case). However, Figs. 4 and 5 also show that background noise for this experiment can produce Bartlett MFP peaks of 0.28 at 10 W and 0.35 at 140 W.

Background noise peaks are caused by at least two phenomena. First, the surface of the test cylinder is mildly excited by the sweep of the hot CO_2 laser beam causing the surface to radiate coherent noise. The test cylinder is centered with respect to the microphone array so this surface noise appears as a false central peak in the Bartlett MFP output in Figs. 4 and 5 for the plug and cylinder case. Second, the rotating mirror assembly, which is centered behind the planar array, hisses at the frequencies of interest while it is in operation. So, just like the cylinder surface noise, the symmetry of this rotating-mirror sound leads to the broad but weak central peak seen in Fig. 3 for 0 W. These noise sources are also discussed in Yönak and Dowling (2002).

IV. CHARACTERISTICS AND SCALING OF PHOTOACOUSTIC SIGNALS

One of the objectives of this research was to determine or at least estimate the sensitivity limit of photoacoustic leak testing. Three features of the photoacoustic signals were examined for their dependence on volumetric leak rate: signal amplitude, signal waveform, and Bartlett MFP peak height. Although the first two signal characteristics are readily measured and amenable to theoretical analyses, the final signal characteristic proved to be the most useful for estimating the sensitivity limit of the present experiments.

A simple scaling law for the photoacoustic signal amplitude can be developed from a little perfect gas thermodynamics and the sound radiation characteristics of compact monopole sound sources. The leaks in this study are presumed to form localized gas clouds whose size is somehow determined by the leak rate and diffusive transport. The

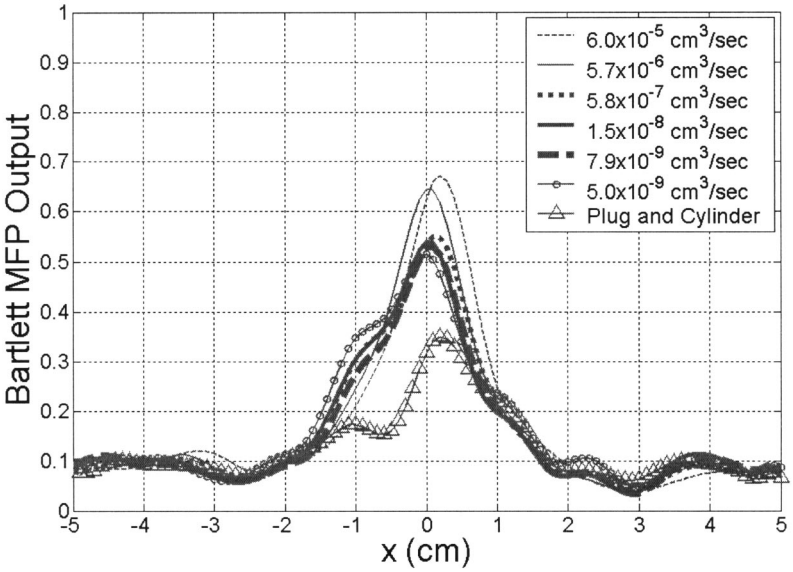

FIG. 5. Same as Fig. 4 except the laser power is 140 W.

amount of photoacoustic sound produced by a gas cloud during a leak test should depend on its size and the characteristics of the swept laser beam. Here, we merely seek to set the parametric dependencies of the sound amplitude. A more comprehensive model of photoacoustic sound production is available in Yönak and Dowling (2003).

In the experiments of this study, photoacoustic sound is generated as the laser beam passes through the tracer gas cloud with volume V, and heats the gas, causing it to expand to size $V+\Delta V$. Assuming that this volumetric expansion is small enough such that the static pressure P is nearly constant, the volume change, ΔV, of the gas cloud is represented by

$$\Delta V = \frac{mR\Delta T}{P} = \frac{mR\Delta E}{Pc_p} = \frac{\gamma - 1}{\rho c^2}\Delta E, \tag{1}$$

and thus will be proportional to the energy, $\Delta E = mc_p\Delta T$, deposited in the tracer gas by the laser beam. In (1), m is the mass of the gas in the cloud, R is the gas constant for the gas in the cloud, c_p is the specific heat at constant pressure for the gas, and γ is the ratio of c_p divided by c_v, the specific heat at constant volume. In addition, the pressure-density (ρ) form of the speed of sound, c, in a perfect gas, $c^2 = \gamma P/\rho$ where ρ is the gas density, has been used to achieve the final equality in (1).

The small volume change specified in (1) is the mechanism that launches the photoacoustic sound. In fact, the volume flux, Q, from an acoustic source is commonly considered to be a measure of its strength (see Kinsler *et al.*, 2000), and the sound amplitude, p, from a monopole is proportional to $\rho f Q/r$, where f is the sound frequency and r is the distance between the source and the listening location. For the present purposes, Q can be approximated by $\Delta V/\Delta t$, where Δt is the time it takes for the laser beam to be swept through the gas cloud. Combining these facts and assuming $f \sim 1/\Delta t$ produces

$$p \propto \frac{\rho f Q}{r} \sim \frac{\gamma - 1}{rc^2(\Delta t)^2}\Delta E. \tag{2}$$

In the present experiments, the gas clouds are much smaller than the laser beam diameter so $\Delta t = d/a$, where d is the laser beam diameter and a is the sweep rate, or speed (in m/s), of the point where the laser beam touches the test surface.

The laser energy deposited in the gas cloud, ΔE, will depend on the laser beam intensity; the length of time that the cloud is illuminated, Δt; the cross section of the gas cloud; the product of the tracer gas absorption constant, β; the laser path length in the gas cloud; and the mole fraction, X, of the tracer gas in the cloud. Here, the laser beam intensity is proportional to W/d^2, where W is the laser power, and the gas cloud cross section and laser path length are taken to be proportional to l^2 and l, respectively, where l is the characteristic size of the gas cloud. These scalings for the cloud cross section and path length presume the cloud to possess nominal spherical symmetry. Thus, the laser energy deposited in the tracer gas cloud should have the following parametric dependence:

$$\Delta E \propto \frac{W\Delta t}{d^2} \cdot l^2 \cdot \beta l X. \tag{3}$$

When (3) and $\Delta t = d/a$ are substituted into (2), a parametric scaling for the amplitude of leak-test photoacoustic sound is obtained:

$$p \propto \frac{(\gamma - 1)Wa}{rc^2 d^3} l^3 \beta X. \tag{4}$$

This scaling law still lacks one important feature: a relationship between the size of the gas cloud, l, and the volumetric leak rate, q. Such a relationship must depend on the mechanisms of tracer-gas mass transport gas away from the leak location. Clearly this might involve the local geometry of the test surface and the type of surface defect from which the tracer gas emerges—a small hole, a crack, a region of porosity, etc. If the leaking tracer gas emerges from a point, the analytic mole-fraction profile derived in Yönak and Dowling (1999) allows the gas-cloud length scale to be set by representative diffusion length. If $R_{1/2}$ is the distance from the point source, where $X = 1$, to the radius where $X = \frac{1}{2}$, then scaling $l \sim 2R_{1/2}$ means

$$l \sim 2R_{1/2} = \frac{q}{\pi D \ln(2)}, \tag{5}$$

where D is the diffusivity of the tracer gas into air ($D \sim 0.1\,\mathrm{cm}^2/\mathrm{s}$ for SF_6 diffusing into air). For the range of leak rates used in this study, (5) produces $l \sim 3\,\mu\mathrm{m}$ at $q = 6 \times 10^{-5}\,\mathrm{cm}^3/\mathrm{s}$, and $l \sim 0.2\,\mathrm{nm}$ for $q = 5 \times 10^{-9}\,\mathrm{cm}^3/\mathrm{s}$. These estimates for l are very small compared to the size of the experimental leak-cap orifice (0.8 mm) which suggests that the geometrical characteristics of the leak may not be well represented by (5). However, use of (5) in (4) leads to the prediction that $p \propto q^3$.

Unfortunately, the experimental results for photoacoustic sound amplitude do not support a cubic dependence on volumetric leak rate. The experiments covered slightly more than four orders of magnitude in q, but the measured signal amplitudes span less than half of the 12 orders of magnitude predicted by a cubic power law. This lack of agreement suggests that the scaling suggested by the combination of (4) and (5) cannot be used to estimate the sensitivity limit of photoacoustic leak testing. The predicted cubic dependence on leak rate comes from assuming that the tracer gas cloud can be characterized by a single length scale, i.e., the cloud is assumed to be nearly spherical. Thus, the lack of scaling-law–experiment agreement suggests that the leak cloud geometry is not nearly spherical but may instead be better modeled as a thin disk lying on the test surface having a planform area set by the leak orifice size with the disk thickness being set by diffusion. Additional understanding of leak cloud geometry requires further investigation and lies beyond the scope of the current effort.

By comparison with the signal amplitude, which did vary with leak rate, the photoacoustic signal waveform was nearly constant for increasing leak rate. Extracting the experimental photoacoustic waveform involved a series of steps in which much of the noise was removed from the

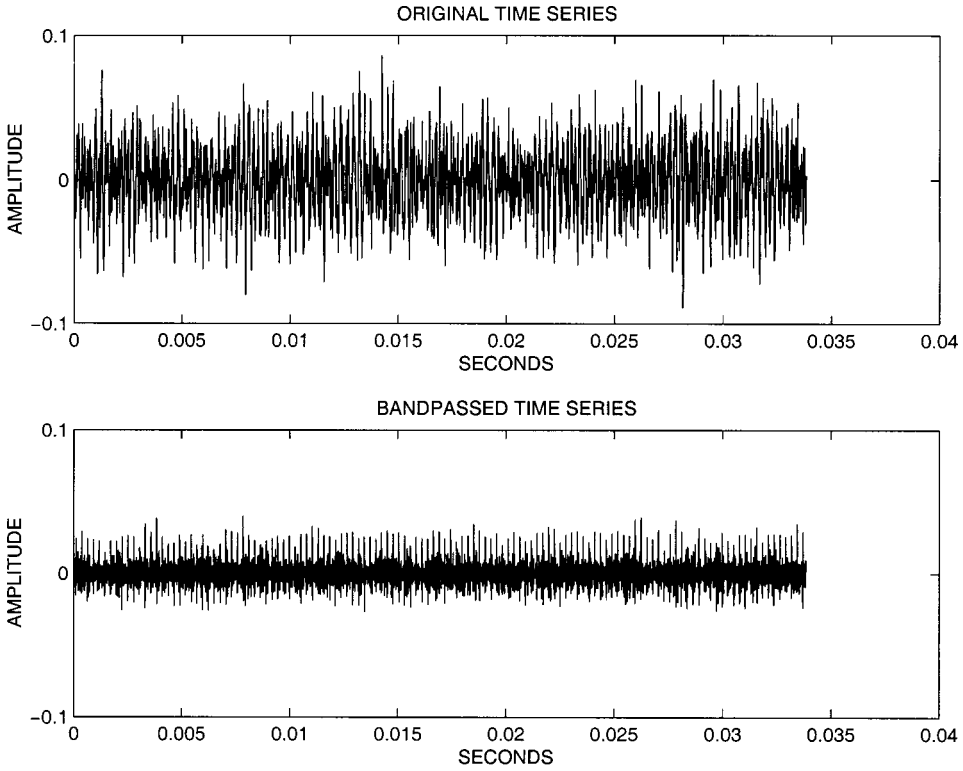

FIG. 6. Time series of measured photoacoustic data with 140 W of laser power scanning the 7.9×10^{-9} cm^3/s leak (top), and the same time series bandpass filtered between 15 and 71.25 kHz. Note the periodicity in the bandpassed time series.

measurements. These steps are illustrated in Figs. 6–8. All of these results were collected by a single microphone with the laser running at 140 W and the $q=7.9\times10^{-9}$ cm^3/s leak mounted on the test cylinder. Figure 6 shows the measured signal versus time for a 34-ms segment of data, and the same segment after bandpass filtering between 15 and 71.25 kHz. The regular periodic spikes seen in the lower panel of Fig. 6 are the photoacoustic signal pulses and four of these are shown with expanded scales in Fig. 7. The letters A, B, C, and D mark direct-path-arrival photoacoustic signal pulse peaks. These peaks actually correspond to negative acoustic pressures because the analog signal electronics of the microphones invert the signal. The temporal spacing between these peaks matches the repetition rate of the laser scan: $\frac{1}{3750}\approx0.267$ ms. The sound measured between the peaks is assumed to be a combination of noise and reflected photoa-

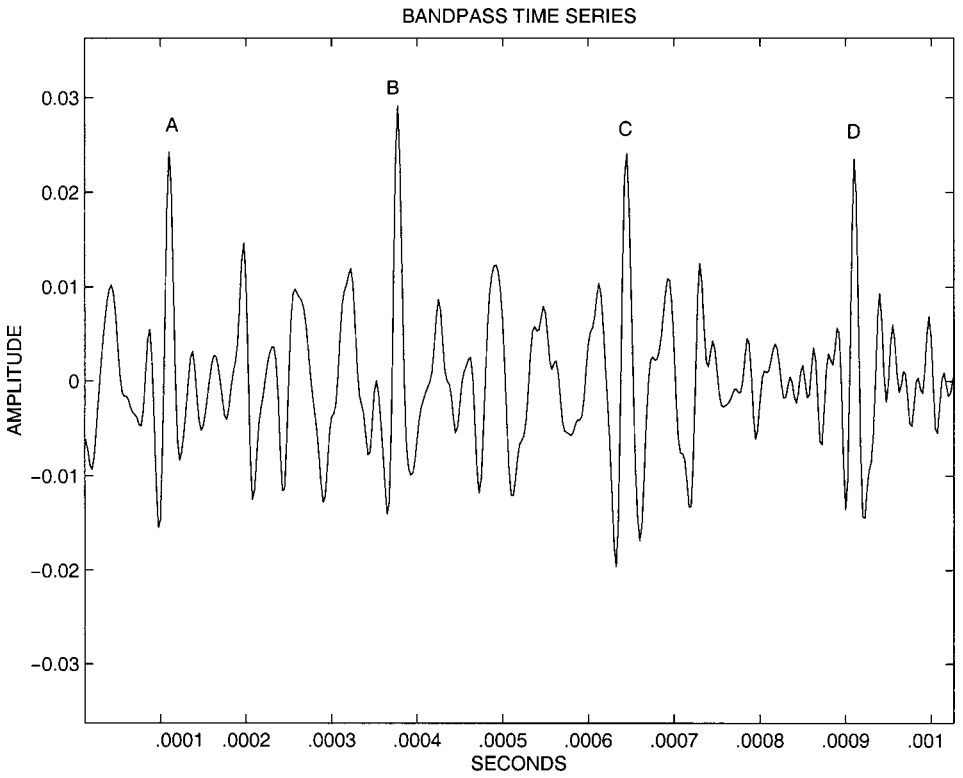

FIG. 7. Bandpass-filtered time series data from the bottom panel of Fig. 6 shown on expanded scales. The letters A–D mark four photoacoustic waveform peaks that occur in the first millisecond of the time series. The positive peaks shown above actually correspond to negative acoustic pressures because the measurements are inverted in the microphone's analog electronics.

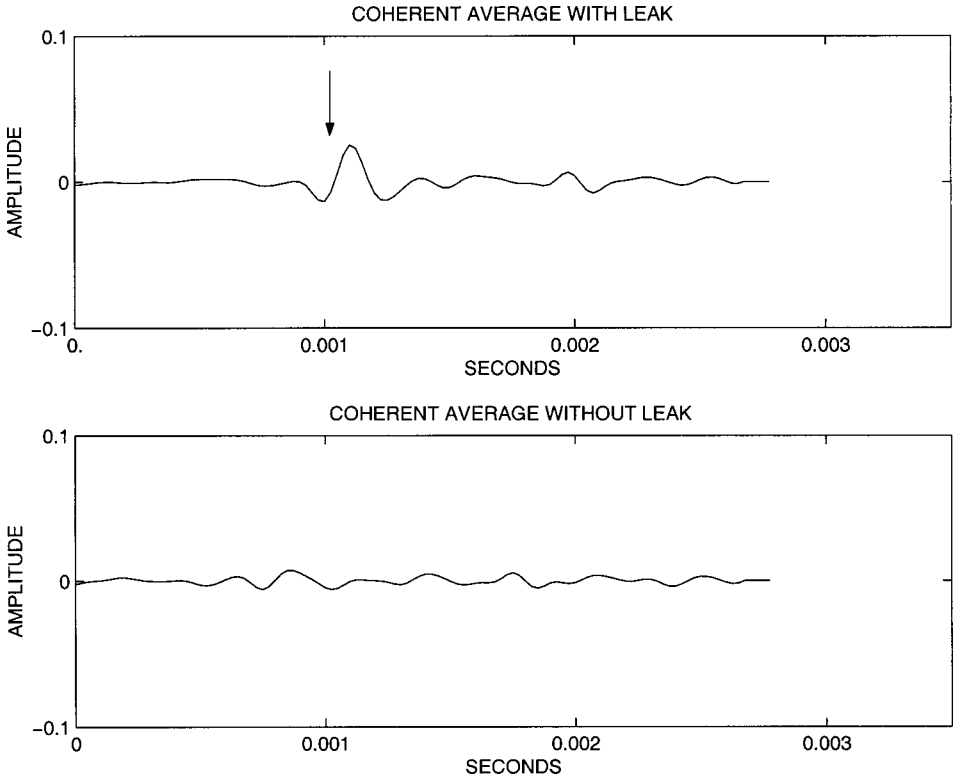

FIG. 8. (Top) Bandpass-filtered time series data from the bottom panel of Fig. 6 coherently averaged over a time window of $\frac{1}{3750}$ of a second. The above results correspond to 126 time windows. The arrow points to the direct-path photoacoustic waveform. It has the same amplitude as the four peaks in Fig. 7, thus it is coherent. (Bottom) Coherently averaged time series results as in the top panel except in this case there is no leak present. An arbitrary and unknown time shift exists between the top and bottom panel.

coustic sounds. In order to assess the extent to which the measured peak and the between-peak sounds were coherent, the measured time series was divided into windows $\frac{1}{3750}$ of a second long and averaged. A sample result of this process is shown in Fig. 8, which was constructed from the 34-ms data segment sample shown in Fig. 6 (upper panel) and an equivalent duration measurement without the leak present (lower panel). An absolute reference to the rotating prism assembly was not available so there is an unknown time shift between the two averaged waveforms in Fig. 8. A comparison of the amplitude levels in Figs. 7 and 8 shows that while the photoacoustic signal level is largely unchanged by averaging, the between-peak sound amplitude is largely suppressed by averaging. This indicates that the photoacoustic signal is coherent while most of the remaining sound (noise) is not. The between-peak sound that is not fully suppressed by averaging, and is thus coherent, is believed to be photoacoustic sound reflected from the optical tabletop and other parts of the experimental environment.

The final means attempted to estimate the sensitivity limit for photoacoustic leak detection was based on the measured MFP peak heights shown in Figs. 3–5. Here, the Bartlett output peak values for each leak at laser powers of 10 and 140 W were plotted versus leak rate and a simple line fit was passed through each set of data as shown in Fig. 9. The leak rates at which these fitted lines cross the measured background-noise-peak level for the same laser power (horizontal lines in Fig. 9) provide an estimate of the sensitivity limit of these photoacoustic leak test experiments. Straight line fits were chosen for this extrapolation task for their simplicity and presumed robustness in the presence of the data scatter shown in Fig. 9. The projected sensitivity limits, $\sim 10^{-11}$ and $\sim 10^{-13}\,\mathrm{cm}^3/\mathrm{s}\,(\mathrm{SF}_6)$ for laser powers of 10 and 140 W, respectively, are not precise and have estimated uncertainties of approximately half an order of magnitude. Even so, while these projected sensitivity limits are certainly impressive, they may yet be quite conservative because they do not account for any noise rejection capability that might be implemented in real applications of photoacoustic technology at these sensitivity levels.

V. SUMMARY AND CONCLUSIONS

A series of demonstration experiments, involving variable laser power and leak rate, have been conducted to estimate the sensitivity limit for photoacoustic leak testing. Three main conclusions can be drawn from this effort. First, the measured results spanning four orders of magnitude in leak rate suggest that the geometry of the tracer gas cloud formed near the leak is nonspherical in nature. Investigating gas cloud shapes and how they influence photoacoustic signal levels appears to be an important future research step. Second, the extrapolated results from the MFP peaks suggest that photoacoustic techniques can provide leak location information while rivaling or even possibly surpassing the sensitivity of conventional helium-mass spectrometry systems for which leak location determination is arduous. However, the implementation details for a photoacoustic leak test system intended to operate in this projected sensitivity range ($q \sim 10^{-11}$ to $10^{-13}\,\mathrm{cm}^3/\mathrm{s}$) will need careful consideration. Past experience has shown that clean test pieces and accurate acoustic models of the test geometry are needed to reject noise and ensure leak localization accuracy. However, novel means of acoustic noise rejection and good metrology may address these concerns. And for the final conclusion, the pho-

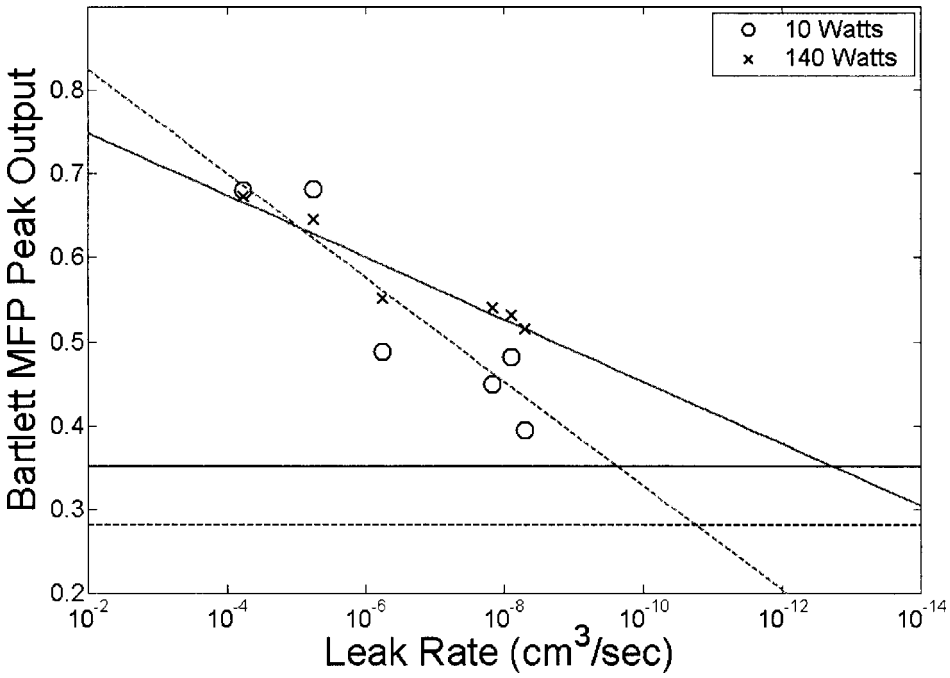

FIG. 9. Extrapolation of the results in Figs. 4 and 5 to smaller leak rates. The sloped lines are fitted to the measured Bartlett MFP peak values. The horizontal lines represent the noise-peak limits. Dashed lines are for a laser power of 10 W. Solid lines are for a laser power of 140 W. The intersection of like lines represents an estimate of the sensitivity limit of the current setup at that laser power. Noise control efforts may extend the sensitivity of the technique to even smaller leak rates.

toacoustic signals from small leaks are coherent so that coherent signal processing techniques can be used to address noise concerns.

ACKNOWLEDGMENTS

This research project was supported by the U.S. Department of Energy through the Kansas City Plant which is operated by Honeywell Federal Manufacturing and Technologies in Kansas City, Missouri. For U.S. Department of Energy under Contract No. DE-ACO4-01AL66850.

Brassington, D. J. (**1982**). ''Photo-acoustic Detection and Ranging—A New Technique for the Remote Detection of Gases,'' J. Phys. D **15**, 219–228.

Dushman, S., and Lafferty, J. M. (**1962**). *Scientific Foundations of Vacuum Technique* (Wiley, New York).

Hablanian, M. H. (**1997**). *High Vacuum Technology: A Practical Guide* (Marcel Dekker, New York).

Jensen, F. B., Kuperman, W. A., Porter, M. B., and Schmidt, H. (**1994**). *Computational Ocean Acoustics* (American Institute of Physics, New York), Chap. 10.

Kinsler, L. E., Frey, A. R., Coppens, A. B., and Sanders, J. V. (**2000**). *Fundamentals of Acoustics*, 4th ed. (Wiley, New York).

McRae, T. G. (**1994**). ''Photo Acoustic Leak Location and Alarm on the Assembly Line,'' Mater. Eval. **52**, 1186–1190.

McRae, T. G., and Dewey, A. H. (**1992**). ''Photo-acoustic leak detection system and method,'' US Patent No. 5,161,408.

Olender, F. T., Woody, B. A., and Newman, L. A. (**1998a**). ''Photoacoustic leak detector with improved signal-to-noise response,'' US Patent No. 5,780,724.

Olender, F. T., Woody, B. A., and Newman, L. A. (**1998b**). ''Photoacoustic leak detector with multiple beams,'' US Patent No. 5,834,632.

Rasmussen, H. H., and Jeppesen., L. (**1998**). ''Industrial Applications of Helium Leak Test,'' NDT.net, Vol. 3, no. 12. (http://www.ndt.net/article/ecndt98/offshore/268/268.htm)

Schroff, G., and Stetter, M. (**1999**). ''Method and apparatus for detecting leaks in a container,'' US Patent No. 5,917,193.

Sharke, P. (**2000**). ''Looking for leaks in all the small spaces,'' Mech. Eng. **122**, 66–68.

Vernonesi, W. A., Olender, F. T., and Hart, R. A. (**2001**). ''Photo-acoustic leak detection system,'' U.S. Patent No. 6,327,896.

Yönak, S. H., and Dowling, D. R. (**1999**). ''Photoacoustic leak detection and localization,'' J. Acoust. Soc. Am. **105**, 2685–2694.

Yönak, S. H., and Dowling, D. R. (**2001**). ''Multiple microphone photoacoustic leak detection and localization system and method,'' US Patent No. 6,227,036.

Yönak, S. H., and Dowling, D. R. (**2002**). ''Parametric dependencies for photoacoustic leak localization,'' J. Acoust. Soc. Am. **112**, 145–155.

Yönak, S. H., and Dowling, D. R. (**2003**). ''Gas-phase generation of photoacoustic sound in an open environment,'' J. Acoust. Soc. Am. (to be published).